Invest New Drugs (2015) 33:835–847
DOI 10.1007/s10637-015-0260-4

PRECLINICAL STUDIES

Three-dimensional and co-culture models for preclinical evaluation of metal-based anticancer drugs

Ekaterina Schreiber-Brynzak[1] · Erik Klapproth[1] · Christine Unger[3] · Irene Lichtscheidl-Schultz[2] · Simone Göschl[1] · Sarah Schweighofer[3] · Robert Trondl[1,4] · Helmut Dolznig[3] · Michael A. Jakupec[1,4] · Bernhard K. Keppler[1,4]

Received: 4 March 2015 / Accepted: 2 June 2015 / Published online: 21 June 2015

Summary *Background* Hypoxic and necrotic regions that accrue within solid tumors in vivo are known to be associated with metastasis formation, radio- and chemotherapy resistance, and drug metabolism. Therefore, integration of these tumor characteristics into in vitro drug screening models is advantageous for any reliable investigation of the anticancer activity of novel drug candidates. In general, usage of cell culture models with in vivo like characteristics has become essential in preclinical drug studies and allows evaluation of complex problems such as tumor selectivity and anti-invasive properties of the drug candidates. *Materials and Methods* In this study, we investigated the anticancer activity of clinically approved, investigational and experimental drugs based on platinum (cisplatin, oxaliplatin and KP1537), gallium (KP46), ruthenium (KP1339) and lanthanum (KP772) in different cell culture models such as monolayers, multicellular spheroids, as well as invasion and metastasis models. *Results* Application of the Alamar Blue assay to multicellular spheroids and a spheroid-based invasion assay resulted in an altered rating of compounds with regard to their cytotoxicity and ability to inhibit invasion when compared with monolayer-based cytotoxicity and transwell assays. For example, the gallium-based drug candidate KP46 showed in spheroid cultures significantly enhanced properties to inhibit protrusion formation and fibroblast mediated invasiveness, and improved cancer cell selectivity. *Conclusion* Taken together, our results demonstrate the advantages of spheroid-based assays and underline the necessity of using different experimental models for reliable preclinical investigations assessing and better predicting the anticancer potential of new compounds.

Keywords 3D models · Metal-based drugs · Anti-invasive properties · Multicellular spheroids · Hypoxia

Abbreviations

CAFs	Carcinoma associated fibroblasts
CC3	Caspase 3
CDDP	Cisplatin
CLSM	Confocal laser scanning microscopy
DAPI	4′,6-diamidino-2-phenylindole
DMSO	Dimethyl sulfoxide
EDTA	Ethylenediaminetetraacetic acid
FCS	Fetal calf serum
FGM	Fibroblast growth medium
GAPDH	Glycerinaldehyd-3-phosphat-dehydrogenase
HFS	Hypotonic fluorochrome solution
HIF1α	Hypoxia-inducible factor 1-alpha
HRP	Horseradish peroxidase
IC50	Half maximal inhibitory concentration
I-OHP	Oxaliplatin
MCR	Multicellular resistance
MEM	Minimum essential medium
PBS	Phosphate buffered saline

Electronic supplementary material The online version of this article (doi:10.1007/s10637-015-0260-4) contains supplementary material, which is available to authorized users.

✉ Michael A. Jakupec
michael.jakupec@univie.ac.at

[1] University of Vienna, Faculty of Chemistry, Institute of Inorganic Chemistry, Waehringer Str. 42, A-1090 Vienna, Austria

[2] University of Vienna, Core Facility Cell Imaging and Ultrastructure Research, Vienna, Austria

[3] Medical University of Vienna, Institute of Medical Genetics, Vienna, Austria

[4] University of Vienna, Research Platform "Translational Cancer Therapy Research", Waehringer Str. 42, A-1090 Vienna, Austria

PBST	Phosphate buffered saline with triton X-100
PI	Propidium iodide
α-SMA	Alpha-smooth muscle actin
STR	Short tandem repeat analysis

Introduction

In the last years, investigations to close the gap between conventional monolayer cell cultures and in vivo models have become of major interest for improving preclinical cancer research and drug development. Efforts ranged from establishment of multicellular spheroids and co-cultivation of spheroids with immune cells to ex vivo cultures of tumor specimens and development of tissue (lab-on-a chip technology) [1] chips. Different 3D culture models, in particular spheroid-based models, have become a useful tool for investigation of specific therapeutic approaches, enhancing the predictive value of drug screening. Monocultures of multicellular spheroids from human tumor cell lines have been reported to mimic in vivo like tumor cyto-architecture, including a proliferation gradient and the presence of hypoxic and necrotic regions with poor nutrition supply [2–4]. This model shows intermediate complexity, still allowing adequate characterization, reproducibility and applicability for drug screenings.

Furthermore, growth of cancer cell lines in spheroids has been reported to cause major changes in gene expression resembling the gene expression patterns in solid tumors, especially with regard to pathways related to cell-cell signaling, cell-cell contacts, cell morphology, cell cycle, and apoptosis induction [5–7]. Moreover, alteration of expression patterns includes genes which are known to play an important role in chemo- and radiotherapy resistance. Additionally, drug sensitivity may be affected by the presence of necrotic and hypoxic regions within the spheroid, analogous to solid tumors in vivo. It has been reported that these regions contain quiescent, non-dividing cells which are insensitive to chemotherapy and radiation [7–11]. Furthermore, drug penetration studies indicated poor drug penetration into the spheroids due to tight cell-cell contacts resulting in multidrug resistance [12] and altered drug metabolism, especially within hypoxic and necrotic regions, corresponding to the in vivo situation [13, 14]. In the past, literature focused mainly on negative selection of drug candidates and reduction of animal studies, implying that the majority of tested drugs lose efficiency in spheroid models [4]. Nevertheless hypoxia, a condition characteristically observed in tumor tissues and enabling metabolic activation of bio-reductive prodrugs, can be a specific target for novel cancer therapy strategies [15].

Additionally, tumor hypoxia has been reported to be associated with tumor invasiveness and metastasis formation in vivo [16, 17], making tumor hypoxia an additional prognostic factor for poor therapeutic outcome [18]. As the mechanisms of hypoxia-driven invasion seem to be similar in spheroid models [19, 20], the latter are an excellent tool to study anti-invasive properties of drug candidates. All these specificities of multicellular spheroid models are opening new opportunities for in vitro drug screenings and enable in vitro studies to address more complex issues, which cannot be solved in 2D culture experiments.

In this study, we compared the anticancer activity of clinically approved, investigational and experimental metal-containing drugs. Therefore, different compounds, based on platinum, gallium, ruthenium and lanthanum, were tested in selected cell culture models, such as monolayers, multicellular spheroids, as well as invasion and metastasis models. Furthermore, we examined the cytotoxicity of the compounds in spheroids with different diameter to get additional insights into whether the presence or absence of hypoxic regions and a necrotic core has an impact on drug efficacy. Moreover, we addressed complex questions by investigating selective targeting of cancer cells in spheroid co-culture with fibroblasts and inhibition of fibroblast mediated invasion. Our work shows how cytotoxicity can tremendously vary depending on the cell culture model applied, whereby it is reasonable to assume that data observed in spheroid models are better approximating the in vivo setting. In total, our results demonstrate the advantages of spheroid-based assays and underline the necessity of using different experimental models for reliable preclinical investigations.

Materials and methods

Cell lines and culture conditions

The human CH1 cell line (identified via STR profiling as PA-1 ovarian teratocarcinoma cells by Multiplexion, Heidelberg, Germany; see also [21]) was kindly provided by Lloyd R. Kelland (CRC Centre for Cancer Therapeutics, Institute of Cancer Research, Sutton, UK). The HCT116 (ATCC® CCL-247™) colon cancer cell line was kindly provided by Brigitte Marian (Institute of Cancer Research, Medical University of Vienna, Austria). Human HT1080 (ATCC® CCL-121™) fibrosarcoma cells and CCD-18Co normal colon fibroblasts were obtained from ATCC (CRL1459) and maintained in FGM (Lonza) supplemented with 2.5 % FCS. Monolayer culture of these cell lines were grown in cell culture treated 75 cm^2 flasks in MEM (supplemented with 10 % heat-inactivated fetal bovine serum (Life Technologies, Austria, Vienna), 1 % L-glutamine, 1 % sodium pyruvate, 1 % non-essential amino acids solution (all from Sigma Aldrich, Vienna, Austria)).

Spheroid formation (3D culture)

For spheroid production, CH1(PA-1), HCT116, and HT1080 cells were harvested from culture flasks by trypsinization and

seeded in MEM (containing antibiotic antimycotic solution with 10,000 units penicillin, 10 mg streptomycin and 25 μg amphotericin B per mL (Sigma Aldrich)) in GravityPLUS™ 96-well plates (InSphero, Zurich, Switzerland) in densities of 1×10^4 (CH1(PA-1)), 2×10^3 (HCT116), and 8×10^3 (HT1080) viable cells/well, respectively, for spheroids with>400 μm diameter 7 days prior to treatment; and in densities of 1×10^3 (CH1(PA-1)), 0.3×10^3 (HCT116), 0.3×10^3 (HT1080) viable cells/well, respectively, for spheroids with<200 μm diameter 3 days prior to treatment. Cultures were maintained at 37 °C in a humidified atmosphere containing 95 % air and 5 % CO_2.

Compounds

Compounds (KP772, KP1339, KP46, KP1537, cisplatin (CDDP) and oxaliplatin (I-OHP) (Fig. 1) have been synthesized at the Institute of Inorganic Chemistry, University of Vienna according to literature procedures [22–27]. KP46 was dissolved in dimethyl sulfoxide (DMSO) to a stock concentration of 20 mM and serial dilutions were prepared in MEM. KP772 and KP1537 were dissolved in MEM to stock solutions of 0.5 mM each and then diluted in MEM to the required concentrations. KP1339 was dissolved in DMSO to a stock concentration of 100 mM and diluted in MEM. Cisplatin and oxaliplatin were dissolved in MEM to a stock concentration of 0.4 mM and diluted further in MEM. All stock solutions were freshly prepared shortly before use.

Confocal microscopy

Thirty spheroids were transferred into 1.5 mL Eppendorf tubes and washed with phosphate buffered saline (PBS, Sigma Aldrich). Samples were then fixed with PBS containing 4 % paraformaldehyde (Sigma Aldrich) and 1 % Triton X-100 (Sigma Aldrich) for 3 h at 4 °C and washed with PBS (three times for 10 min). An ascending methanol series was used for dehydration at 4 °C in PBS (25 %, 50 %, 75 %, 95 % for 30 min each and 100 % for 3 h), and the reverse methanol series were used for rehydration. Samples were washed with PBS (three times for 10 min). Samples were blocked and permeabilized with PBST (0.1 % Triton X-100 in PBS containing 3 % bovine serum albumin (Sigma Aldrich)) overnight at 4 °C, subsequently washed twice for 15 min with PBST and incubated for 48 h at 4 °C with HIF1α antibody (Abcam, Cambridge, UK) diluted 1:400 in PBST. After washing four times for 30 min with PBST, secondary antibody - Alexa Fluor 647 (Cell Signaling, Frankfurt am Main, Germany) diluted 1:1000 in PBST was added for 24 h at 4 °C. Samples were finally washed four times for 30 min in PBST and investigated with a confocal microscope Leica CLSM (Leica Microsystems, Wetzlar, Germany).

Propidium iodide staining

Viable spheroids were transferred into a Falcon non-tissue culture treated u-bottom 96-well plate, one spheroid per well in a total volume of 40 μL MEM (supplemented with 10 % heat-inactivated fetal bovine serum (Life Technologies), 1 % glutamine (Sigma Aldrich), 1 % sodium pyruvate (Sigma Aldrich), 1 % non-essential amino acids solution (Sigma Aldrich)). One hundred sixty microliter propidium iodide (Sigma Aldrich) diluted in MEM to a final concentration of 1 μg/mL were added per well. Samples were incubated for 8 h at 37 °C, 5 % CO_2 prior to image acquisition.

Fluorescence microscopy

For analysis of fluorescent properties, a confocal laser scanning microscope CLSM from Leica (Leica SP5) was used. It was equipped with 2.5×, 10× and 20× multiimmersion objectives for low magnification, and for high magnification with 40× and 60× oil, water and glycerol objectives. Tonal range adjustment of the micrographs was carried out in Adobe Photoshop CS 4.

Cell cycle analysis

Spheroids were harvested and transferred into 1.5 mL Eppendorf tubes, washed with 1 mL PBS (Sigma Aldrich) and treated with 300 μL 0.25 % trypsin-EDTA solution (Sigma Aldrich) for 7 min to obtain a single-cell suspension. The trypsin-EDTA solution was inactivated by adding of 300 μL MEM. Cells were pelleted by centrifugation, washed with PBS (1×) and resuspended in 600 μL PI (50 μg/mL) /HFS (hypotonic fluorochrome solution: 0.1 % (*v/v*) Triton X-100, 0.1 % (*w/v*) sodium citrate, in PBS) solution. After overnight staining at 4 °C samples were analyzed with a flow cytometer (Guava easyCyte 8HT, Millipore, Austria, Vienna).

Alamar Blue assay

For tests with monolayers, CH1(PA-1), HCT116, and HT1080 cells were harvested from culture flasks by trypsinization and seeded in MEM into 96-well microculture plates (Falcon) 24 h prior to treatment in densities of 1×10^3 (CH1(PA-1)), 2×10^3 (HCT116), 3×10^3 (HT1080) viable cells/well, respectively.

For tests in 3D cultures, spheroids with the required diameter were transferred into Falcon non-tissue culture treated u-bottom 96-well plates shortly before drug treatment. As the spheroid harvest volume was 40 μL, 60 μL of MEM were added per well prior to treatment.

For both monolayer and spheroid treatment, stock solutions of the test compounds were prepared and diluted stepwise to obtain a gradient dilution row. One hundred microliter of

dilution were added to each well, and plates were incubated for 96 h at 37 °C and 5 % CO_2. A fresh solution of 440 μM (≈110 μg/mL) resazurin sodium salt (Sigma Aldrich) in PBS was prepared, and 20 μL of it were added to each well. Plates were stained at 37 °C and 5 % CO_2 for 4 h (monolayer experiments) or overnight (spheroid experiments).

Transwell invasion assay

The transwell assay was performed according to a protocol described by other authors [28]. In detail, growth factor reduced Matrigel (BD, Heidelberg, Germany) was defrosted on ice and diluted in 4 °C PBS to a final concentration of 300 μg/mL. Fifty microliter of the dilution were added to each insert of a cell culture insert companion plate (BD) with 8 μm pore size and incubated overnight at 37 °C. Prior to use inserts were rehydrated for 1 h at 37 °C by adding of 700 μL serum-free MEM (Sigma Aldrich). HT1080 cells were grown in Cyto One T75 flasks to subconfluence of ~80 %. Cells were harvested, counted and diluted in serum-free MEM (Sigma Aldrich) to a final density of 3.75×10^5 cells per mL. Appropriate drug concentrations were added to the cell suspension to achieve sub-cytotoxic effects. Two hundred microliter of cell/drug suspensions were added to each invasion chamber in 24-well plates. Seven hundred microliter of chemoattractant (MEM with 10 % FBS, 1 % glutamine) were added via the access port. Cell invasion chambers were incubated overnight at 37 °C under a humidified atmosphere containing 95 % air and 5 % CO_2. MEM was aspirated from the inserts, and Matrigel remains and non-invaded cells were removed with a MEM-moistened cotton swab. Inserts were then transferred in new 24-well plates, and 100 μL of trypsin-EDTA solution (Sigma Aldrich) were added via the access port. After 5 min incubation at 37 °C, inserts were removed and cells harvested with 100 μL MEM. Cell samples were immediately stained with Guava ViaCount Flex Reagent (Millipore) for 5 min at RT and measured with a flow cytometer (Guava easyCyte 8HT, Millipore).

Spheroid invasion assay

Spheroids were grown to a diameter of 400–450 μm (see below), then transferred into a Falcon non-tissue culture treated u-bottom 96-well plate, with one spheroid per well in a total volume of 40 μL MEM. One hundred twenty microliter of Matrigel diluted in MEM to a final concentration of 300 μg/mL were added to each well. If required, drugs in subcytotoxic concentrations were added to MEM prior to Matrigel dilution. After 96 h samples were analyzed with an inverted culture microscope (Olympus), CKX41 (4× objective) and ImageJ software. For fibroblast invasion CCD-18Co cells were seeded into a u-shape 96-well plate at 500 cells/well in FGM containing 20 % methylcellulose, centrifuged (200 g, 5 min) and incubated until proper spheroid formation (5 h). Spheroids were embedded in 300 μl collagen I gel as described above, and then FGM containing KP46 (7.5 μM) or KP772 (1 μM) was added. Invasion of fibroblasts into the collagen matrix was documented by bright field microscopy imaging after 7 days.

Spheroid invasion was also visualized with a JuliBR live cell monitor system (NanoEntek, Seoul, Korea). Untreated and treated samples were monitored in parallel with measurement of the cross-sectional area every hour over an overall time period of 96 h.

Spheroid co-culture assay

This method was described in detail in Dolznig et al., 2011. In brief, 500 HCT116 cells/well were seeded into a u-shape 96-well plate in MEM/5 % FCS (Sigma Aldrich) containing 3 % methylcellulose and allowed to aggregate for 48 h. For one gel, 48 spheroids together with 3×10^5 CCD18-Co fibroblasts were embedded into 300 μl collagen I matrix (final conc. 2 mg/mL, #354236, Corning B.V., Corning, USA). After solidification, 3 mL DMEM (10% FCS) and compounds (KP46 7.5 μM, KP772 1 μM) were added, and the gels were incubated for 72 h and subsequently fixed in Histofix (Lactan, Graz, Austria). To assess cell viability, gels were stained for cleaved caspase 3 (rabbit mAB, Cell Signaling, #9661 and anti-rabbit Alexa Fluor 488) according to manufacturer protocol for immunofluorescence followed by confocal imaging on a Leica DM6000 CFS fixed stage microscope (Leica Microsystems, Wetzlar, Germany) using a 20× objective (NA=1.32). DAPI served as nuclear counterstain.

Collagen gel contraction assay

To evaluate the contractile capacity of fibroblasts under treatment, 3×10^4 CCD-18Co cells were embedded into 300 μl of a collagen I matrix (2 mg/mL). After solidification, 3 mL MEM (10 % FCS) with or without KP46 (7.5 μM) were added. Gels were photographed daily for 7 days, and the size of the collagen gels (projected surface area) was determined by ImageJ software analysis. Additionally, fibroblast viability was assessed by the Alamar Blue assay.

Western blot studies

The expression level of α-SMA was evaluated with a monoclonal mouse anti-human smooth muscle actin, clone 1A4 antibody (Dako, 1:1000). As loading control, the housekeeping gene GAPDH was used and detected with rabbit anti-human GAPDH (14C10) antibody (Cell Signaling) in dilution 1:1000. Secondary antibodies anti-mouse IgG, HRP-linked antibody (Cell Signaling) and anti-rabbit IgG, HRP-linked antibody (Cell Signaling) were used in dilution 1:1000.

Western blot studies were performed in two independent experiments. Samples were treated for 18 h prior to protein isolation with KP772 in concentrations of 1 and 2 μM and with KP46 in concentrations of 7.5 and 15 μM.

Statistical analysis

For statistical analysis, an unpaired *T*-test with Welch's correction from raw data was performed. All results are based on at least three independent experiments.

Results

Characterization of the spheroid model

We used the hanging drop technique for growth of spheroids with diameters of <200 and >400 μm. This method allowed us to grow single spheroids per well in the 96-well format with a proper control of spheroid size. The used cell lines HCT116 (colon carcinoma), CH1(PA-1) (ovarian teratocarcinoma) and HT1080 (fibrosarcoma) were previously described in the literature to form compact, round shaped spheroids [29–31].

To evaluate the influence of 3D growth on the cell lines, we performed cell cycle studies with both spheroids and monolayer cultures. Cells from monolayer culture were ~80 % confluent prior to harvesting for better comparison within the experiments. In agreement with previously published results [32], our cell cycle studies showed a decreased fraction of S phase in both spheroid sizes of all tested cell lines (Fig. 2a), indicating the presence of an increased population of non-dividing cells. In monolayer culture the number of cells in S phase was four times higher than in spheroids, which corresponds to a decelerated, but still well detectable population of proliferating cells (Fig. 2a).

Since hypoxic regions and necrotic core are main characteristics of spheroid models and can play a crucial role in drug screening outcome, we confirmed the presence of a necrotic core by propidium iodide staining in viable spheroids and the presence of hypoxic regions by antibody staining of HIF1α in whole spheroids fixed with formaldehyde solution. Presence of HIF1α has been previously reported in all types of hypoxic cells [33, 34] as an early cell response to low oxygen supply. Due to this observation, determination of the protein level of HIF1α is commonly used for characterization of hypoxia in solid tumors and hypoxic cell culture models. Due to limited penetration ability of the argon laser, CLSM investigations were done at the maximum depth of 70–80 μm. Our results illustrate the presence of both a necrotic core and a hypoxic region in spheroids with >400 μm diameter, but not in smaller spheroids with less than 200 μm diameter (Fig. 2b and supplementary data Fig. 1). Furthermore, the hypoxic region appears in ring form and is located already at the depth of 30 μm under the spheroid surface, while the inner core of the spheroid showed persistent massive necrosis.

Cytotoxicity in spheroids with and without hypoxia

We evaluated the cytotoxic effects of different metal-based compounds, some of which (cisplatin and oxaliplatin) are approved and frequently used anticancer agents. The gallium (KP46) and ruthenium (NK1339) based compounds have already been successfully evaluated in phase I clinical trials [35–37] and are promising candidates for future clinical use.

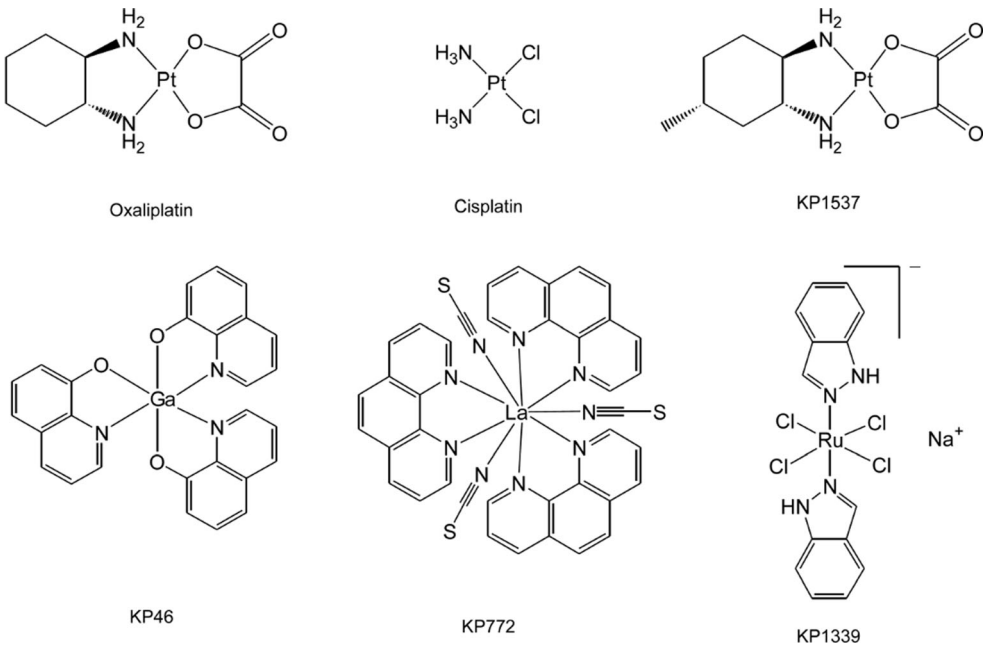

Fig. 1 Structural formulas of compounds used in this study

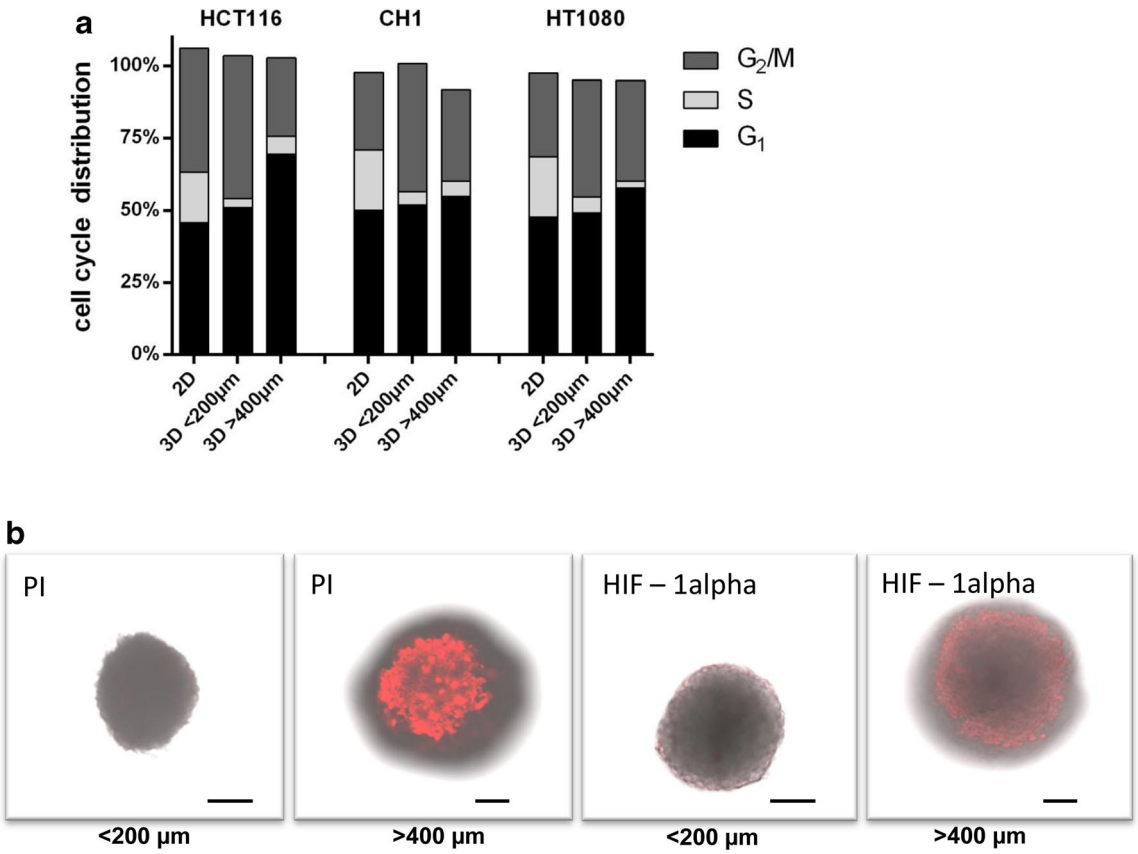

Fig. 2 Characterization of spheroids with different diameters. **a**. Cell cycle distributions in HT1080, HCT116 and CH1(PA-1) spheroids with diameters of <200 and >400 μm compared to monolayer cultures. **b**. PI staining of the necrotic core and immunohistochemical detection of HIF1α expression in HT1080 spheroids with <200 and >400 μm diameter. *Grey areas* depict total spheroid size. Scale bars 100 and 50 μm, respectively

We also included experimental platinum (KP1537) and lanthanum (KP772) based compounds, developed in our lab. The studied compounds show different chemical and biological properties. KP46 is not redox active under physiological conditions but shows high in vitro cytotoxicity, whereas KP1339 is a redox active drug, but was found to be less active in vitro. Choosing compounds with such diverse chemical and biological properties and in different stages of clinical and preclinical development allowed us to scrutinize our 3D culture models and investigate the dependence of cytotoxicity on the cell model used for screening.

Cytotoxicity of platinum (KP1537), gallium (KP46), ruthenium (KP1339) and lanthanum (KP772) based compounds was tested on spheroids with and without hypoxic regions and necrotic core and on monolayers of HCT116, CH1(PA-1) and HT1080 cells by using the Alamar Blue assay. Three of four compounds tested in spheroids with <200 and >400 μm diameter showed a spheroid size dependent increase of IC_{50} values (Fig. 3a). In contrast, the IC_{50} values of KP772 in spheroids are well comparable with those in monolayer culture.

Detailed comparison of data obtained for all tested substances, including the standard drugs cisplatin and oxaliplatin, in >400 μm spheroids and monolayers show that use of the 3D model results in a totally new ranking of compounds with regard to their cytotoxicity in vitro (Fig. 3b). Remarkably, cisplatin, oxaliplatin, KP772 and KP1339 showed no tremendous changes in cytotoxic potency in <200 or >400 μm spheroids, whereas the cytotoxicity of gallium complex KP46 and oxaliplatin derivate KP1537 was markedly lower in the hypoxic spheroid model. Especially KP46, yielding IC_{50} values in the low micromolar range in monolayer culture, showed a 300-fold decrease of cytotoxicity in >400 μm spheroids (Fig. 3a).

Anti-invasive activity in spheroid model and transwell assay

Hypoxic tumors in vivo show a tendency to metastasize, which is the most common cause for rapid disease progression and lethal disease outcome. Therefore, establishment of in vitro models for invasiveness and drug screenings for anti-invasive activity should be considered essential for preclinical investigations. We evaluated the anti-invasive properties of the investigated compounds in different assays, such as a transwell assay (evaluating the influence on migration ability and invasiveness in cell monolayers) and a spheroid-based assay (studying the ability of the compounds to inhibit the

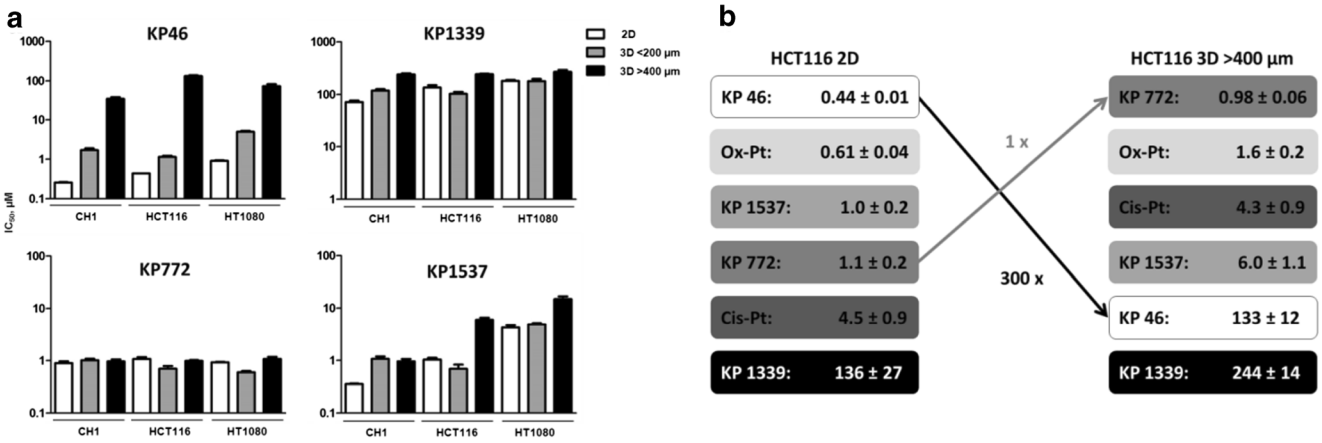

Fig. 3 Cytotoxicity of the tested compounds in spheroids with <200 and >400 µm diameter and monolayer cultures. **a**. IC_{50} values (means± standard deviations) in monolayers, hypoxic and non-hypoxic spheroids of CH1(PA-1), HT1080 and HCT116 cells. **b**. Ranking of the compounds by IC_{50} value in HCT116 monolayers and hypoxic spheroids

formation of metastasis-like protrusions). The transwell assay was carried out for 24 h in HT1080 cells. The number of invaded cells was evaluated by flow cytometric analysis, which additionally allowed the monitoring of cell viability. The spheroid assay was carried out for 96 h with hypoxic HCT116 and HT1080 spheroids. Spheroid invasion was evaluated by microscopy after 96 h. Due to their highly invasive properties, HT1080 cells were used for the transwell assay. Growth of HCT116 spheroids containing a hypoxic zone and a necrotic core increased the invasiveness of this cell line, rendering HCT116 suitable for the spheroid-based assay (see supplementary data Fig. 2). Applied compound concentrations were proven to be in the subcytotoxic range for the chosen incubation period.

In accordance with results of our cytotoxicity screening, most compounds (cisplatin, oxaliplatin, KP1339, and KP1537) displayed higher anti-invasive properties in the monolayer-based transwell assay. However, KP772 and KP46 showed high anti-invasive properties in the spheroid model. Moreover, KP46 was the only compound which displayed a higher anti-invasive activity in the spheroid invasion assay. KP46 had significant anti-invasive activity in both HT1080 (Fig. 4a,c and Electronic supplementary material) and HCT116 spheroids (see supplementary data Fig. 2), inhibiting appendage formation and spheroid growth. KP772 displayed high anti-invasive activity in the transwell assay and was moderately inhibiting invasion in the spheroid-based assay (Fig. 4b). While a related compound investigated previously [38] caused significant reduction of cell migration and invasion in breast cancer cell lines, the ruthenium complex KP1339 had no anti-invasive activity in the models applied here. KP1537 and oxaliplatin, with significant activity in the transwell assay, were inactive in the spheroid invasion assay. Cisplatin, being inactive in the transwell assay, showed slightly increased activity in the spheroid-based assay.

As KP46 and KP772 significantly inhibited invasion in the spheroid-based model, we monitored the protrusion formation in hypoxic HT1080 (Fig. 5a and b) and HCT116 (data not shown) spheroids for 96 h. For this purpose, images and measurements of the cross-sectional area were made automatically every hour. Both KP46 and KP772 caused inhibition of protrusion formation already after ca 21 h (Fig. 5a and b).

KP46 inhibits normal fibroblast mediated invasion and contraction of collagen gels

In order to test whether KP46 has anti-invasive effects on carcinoma associated fibroblasts (CAFs) isolated from colon carcinomas [39], we employed the spheroid collagen gel invasion assay using CCD18-Co myofibroblasts as a model resembling activated colon cancer fibroblasts. Indeed, after 168 h of culture in collagen gel, KP46 treated cultures showed no signs of invasion as compared to DMSO controls and KP772 treated samples (Fig. 6a). Importantly, the fibroblasts were not affected in the presence of KP46 or KP772 as determined by morphology in transmission light microscopy. Consistent with the non-invasive phenotype upon KP46 treatment, no signs of gel contraction were detectable (Fig. 6b), whereas DMSO controls showed prominent gel shrinkage. Determination of the projected area revealed a threefold reduction of collagen gel size under control conditions, whereas under treatment with KP46 the collagen gels contracted only to about 85 % of their initial size (Fig. 6c). Of note, no severe reduction of cell viability was detectable in KP46 treated fibroblasts in the contracted collagen gels after 7 days of treatment (Fig. 6d).

Alpha-smooth muscle actin expression has been proven by other authors to have a direct impact on contractile activity of fibroblasts [40] and to be associated with invasive activity of different cancer types [41, 42]. To evaluate whether the loss of contractile activity and invasion in Cav18Co fibroblasts under

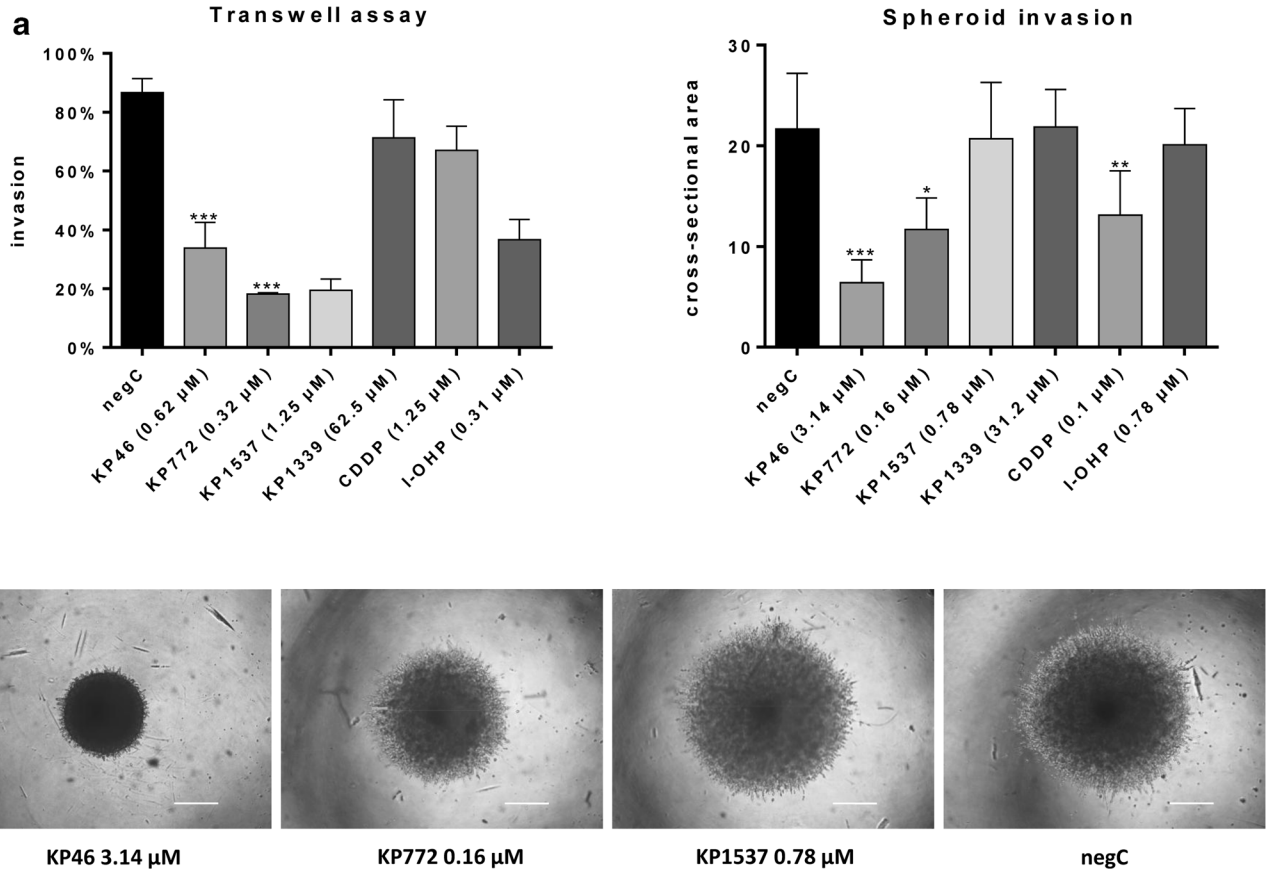

Fig. 4 Anti-invasive activity of the investigated compounds. **a**. Comparison of anti-invasive activity in the spheroid model and the transwell assay in the cell line HT1080. **b**. Inhibition of protrusion formation in HT1080 by KP46, KP772 and KP1537. Significantly different to control by *T*-test with Welch's correction *** $p<0.001$, ** $p<0.01$, * $p<0.05$. Scale bar 200 µm

KP46 treatment are associated with alpha-smooth muscle actin expression, we performed Western blot studies. Indeed, KP46 decreased smooth muscle actin level in a dose-dependent manner, while KP772 has no influence on protein expression (Fig. 6e). Further, our observations showed time-dependent morphology changes and detachment of the fibroblasts in presence of KP46.

Selective targeting of colon cancer cell spheroids by KP46

Next we determined the effects of KP46 and KP772 in an organotypic 3D model recapitulating tumor–stroma interaction. For this purpose, HCT116 spheroids were embedded into fibroblast containing collagen I and incubated for 3 days in the presence or absence of KP46 or KP772. After 48 h no obvious signs of cell death were detectable by light microscopy, whereas after 72 h a profound effect was seen in the KP46 treated cultures. The spheroids appeared less compact, and invasive structures were reduced in the KP46 containing cultures (Fig. 7a). The gels were subsequently fixed and subjected to immunofluorescence staining for cleaved caspase 3 (CC3) and confocal imaging. Massive apoptosis was induced in the tumor cell spheroids under KP46 treatment, whereas KP772 showed intermediate effects as compared to DMSO treated controls, which showed only sporadic apoptotic features (Fig. 7b and supplementary data Fig. 3). In good accordance with our previous findings, no signs of apoptotic fibroblasts were detectable in KP46 treated samples, whereas KP772 treatment elicited minor cell death in the mesenchymal cells.

Discussion

In this study, we used alternative cell culture models to investigate anti-tumoral and anti-invasive properties of gallium, platinum, ruthenium and lanthanum-based compounds in different cell culture models: monolayers, hypoxic and non-hypoxic cancer cell spheroids, fibroblast spheroids and fibroblast/cancer cell co-culture. The application of these models in combination with invasion assays allowed us to provide novel insights into the mechanisms of action of the studied drugs.

The gallium-based compound KP46, which had already shown signs of therapeutic activity in patients with renal cell cancer in a clinical phase I study [35], showed the strongest

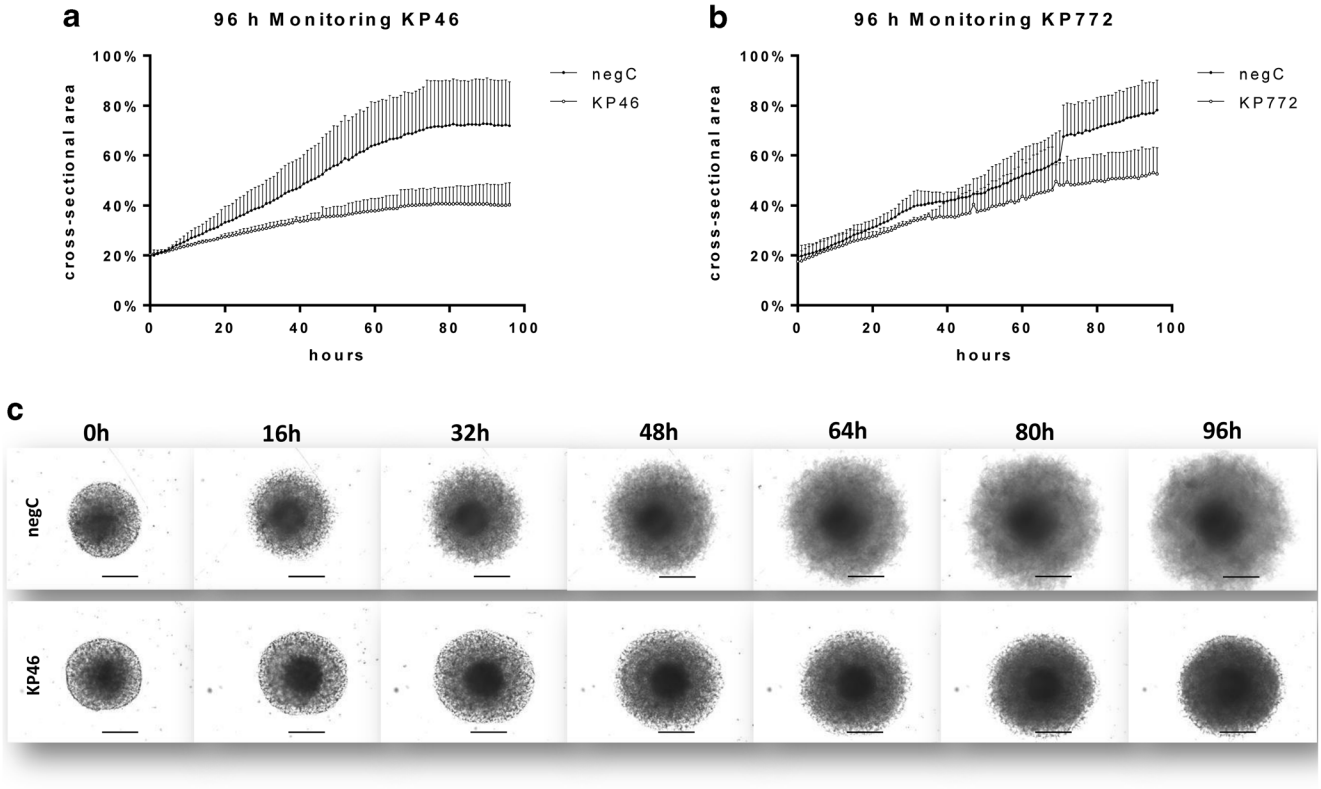

Fig. 5 Ninety six hours monitoring of anti-invasive activity of KP46 and KP772 in the hypoxic HT1080 spheroid model by a JuliBr system. **a**. KP46 and **b**. KP772 time-dependent anti-invasive activity. **c**. Selection of images showing inhibition of protrusion formation due to KP46 treatment over 96 h. Scale bar 200 μm

dependence of both cytotoxicity and anti-invasive activity on the used culture models. In monolayer culture, IC_{50} values were in the low micromolar range for all three cell lines used in this study, which is in good accordance with results published previously [43]. Corresponding to experience in animal studies and the clinical trial where the dose of KP46 had to be escalated to higher levels than expected, we observed a strong decrease in cytotoxic activity (~300-fold) in spheroid culture compared to the monolayer model. This seems to be in contrast to a previous report [44], which, however, involved cells with a certain degree of intrinsic resistance to KP46, according to the two-digit micromolar IC_{50} values given there even for the monolayer setting. It is well known that three-dimensional cell culture models mimicking a solid tissue environment are frequently showing decreased drug sensitivity, a phenomenon called multicellular resistance (MCR) by some authors [44]. The main reasons for the development of MCR are cell cycle changes, in particular a low fraction of dividing cells [45], decreased drug penetration due to tight cell-cell contacts and cell-matrix interactions [46], and, if present, hypoxia may contribute to resistance by inducing changes in expression of apoptosis regulators [47]. With regard to drug penetration, extracellular binding of the drug to macromolecules such as serum albumin [48] might constitute another obstacle. However, if this were a relevant factor in the case of KP46, the same should apply to other compounds with affinity for albumin, such as KP1339, contrary to our observations.

In further contrast, KP46 showed low anti-invasive activity in the monolayer-based transwell assay, whereas it strongly inhibited protrusion formation in the spheroid-based invasion assay. An explanation for these results could be differences in expression levels of adhesion molecules between spheroid culture and monolayer culture. Cells grown in spheroids are known to produce increased amounts of adhesion molecules [49], which in general mediate invasiveness. KP46 has been reported recently to down-regulate focal adhesion proteins, in particular integrin-b1, causing deregulation of cell-matrix adhesion [50]. In good agreement with these findings, we showed that KP46 inhibits contraction of collagen I gels by fibroblasts and fibroblast invasion into collagen I, corroborating the impact on stroma interactions caused by treatment with this compound. We showed further that KP46 down-regulates α-SMA in monolayer culture of fibroblasts in a dose-dependent manner, which can be an additional reason not only for the anti-invasive activity of the compound, but also for cell morphology changes and cell detachment observed in fibroblasts (see Electronic supplementary material) and cancer cell lines [50]. Data obtained from HCT116/fibroblast co-culture in a 3D matrix, however, showed that KP46 selectively targets cancer cells but has no discernible impact on fibroblast

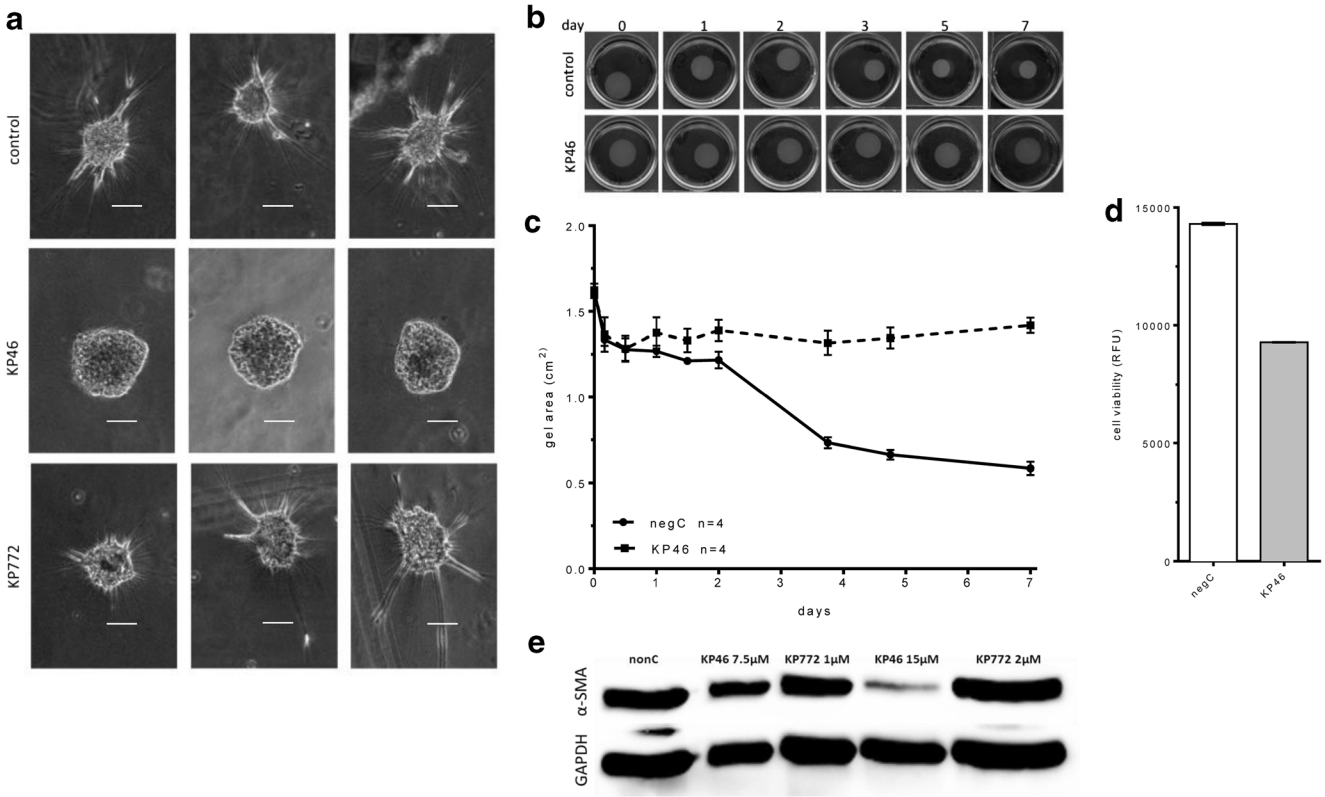

Fig. 6 KP46 impairs mobility and contractile force of normal colon fibroblasts in a collagen I matrix. **a**. Fibroblast invasion into collagen I gel after 7 days of treatment with KP46 (1 μM), KP772 (7.5 μM) or DMSO (control). **b**. Contraction of collagen I gels by fibroblasts treated with KP46 (1 μM) or DMSO (control) monitored for 7 days. **c**. Gel areas of B analyzed in ImageJ. **d**. Viability of cells in contracted gels analyzed by the Alamar Blue assay. **e**. Down-regulation of α-SMA in fibroblast monolayer culture shown by Western blotting. *Error bars* indicate±SD. Scale bar 100 μm

viability. Results of KP46 with spheroid models suggest that KP46 is a potent inhibitor of tumor invasion but might be cytotoxic primarily to proliferating rather than quiescent cancer cells.

In contrast to KP46, there is little difference between the anti-cancer activities in monolayer culture or spheroids in the case of the lanthanum-based compound KP772. Cytotoxicity tests showed similar IC_{50} values in both spheroid and monolayer culture, indicating that multicellular resistance has no impact on compound activity. As the anticancer activity of KP772 involves a strong cell cycle arrest [51], it was reasonable to expect a decrease of cytotoxicity in spheroid culture, which was not the case, however. Alternatively, the activity of KP772 might hardly be inhibited by hypoxia in contrast to that of KP46 (W. Berger, personal communication). On the other hand, KP772 showed high anti-invasive activity in the monolayer-based transwell assay but moderate anti-invasive activity in the spheroid-based assay. Corresponding with this observation, treatment with KP772 had no impact on fibroblast invasion, but showed cytotoxicity to fibroblasts in HCT116/fibroblast co-culture, suggesting a lower selectivity for tumor cells than KP46.

Cytotoxic or anti-invasive properties of the ruthenium-based compound KP1339 showed very little dependence on the cell model used. Surprisingly, treatment with KP1339 yielded similar IC_{50} values in monolayers and hypoxic as well as non-hypoxic spheroids. This finding is rather unexpected, taking into consideration the activation-by-reduction hypothesis which is a central aspect in the rationale for the development of anticancer ruthenium(III) complexes [52]. According to this hypothesis, ruthenium(III)-based compounds serve as pro-drugs being activated in the hypoxic milieu of the solid tumors. Animal studies in mice with KP1339 showed significant anti-tumor activity in vivo [53], and in a phase I clinical trial about one third of the patients treated with therapeutically relevant doses showed either disease stabilization or a partial response, most notably those with gastrointestinal neuroendocrine tumors [37]. This would not be anticipated based alone on the cytotoxicity in monolayer cultures, which is in fact rather low. Nevertheless, a correlation between normoxia versus hypoxia and cytotoxic activity of KP1339 has never been reported. Another possible explanation for increased cytotoxicity in vivo is albumin-mediated uptake [54, 55]. Previous studies regarding the anti-invasive activity of ruthenium-based compounds revealed certain anti-invasive activity of

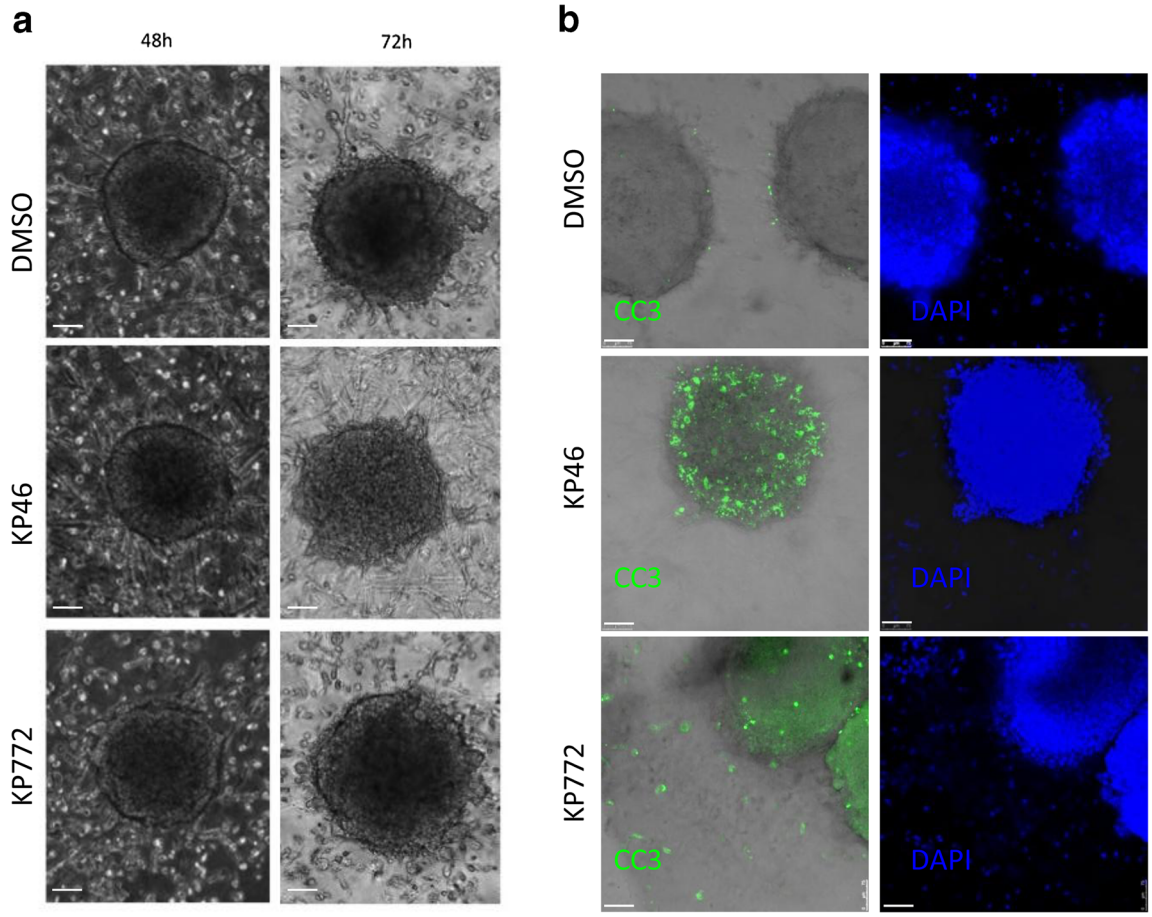

Fig. 7 Spheroid co-culture in a collagen I matrix reveals tumor cell selective apoptotic action of KP46. **a**. Bright field microphotographs of treated (KP46 1 μM, KP772 7.5 μM) co-cultures. **b**. Confocal immunofluorescence images of pro-apoptotic cleaved caspase 3 and DAPI as nuclear counterstain. Scale bar 75 μm

KP1019, a KP1339 analogue, in monolayer cultures of breast cancer cell lines [38]. Our results, however, could not demonstrate anti-invasive activity of KP1339, neither in the transwell nor in the spheroid-based assays.

The biological activities of KP1537, an oxaliplatin analogue, showed a pronounced dependence on the cell model used, indicating both decreased cytotoxicity in hypoxic spheroid models and decreased anti-invasive activity in the spheroid-based invasion assay. These results are paralleled by those for oxaliplatin included in this study. They also correspond with findings published by other authors, who reported a decrease of oxaliplatin sensitivity with depth in HCT116 spheroids and revealed a clear gradient of drug penetration, induced DNA damage and HIF1 activity [56]. Moreover, these authors observed that the difference in sensitivity to oxaliplatin between cells from normoxic vs hypoxic regions (8-fold) exceeded the differences in DNA platination (1.5-fold), suggesting that hypoxia-triggered molecular changes have a stronger impact than penetration issues, which was supported by reduced resistance in spheroids of a subline lacking functional HIF1 (the master regulator of hypoxia response). This corresponds to our finding that cytotoxicity of the oxaliplatin analog KP1537 is in two (of three) cell lines only affected in larger spheroids displaying HIF1α expression.

In summary, especially KP46 showed strong differences depending on the culture model used, while other compounds used in this study, such as KP1537 and oxaliplatin, displayed moderately different, or, like KP772, KP1339 and cisplatin, rather comparable cytotoxicity in all used culture models. All compounds, except for cisplatin, included in this study showed anti-invasive properties in the transwell assay, most notably KP772, KP1537 and oxaliplatin. In the spheroid-based assay, however, only KP46, cisplatin and KP772 had anti-invasive activity, and only KP46 and cisplatin showed increased anti-invasive activity compared to the transwell assay.

In general, our findings suggest that cytotoxicity and anti-invasive activity are very much dependent on the cell culture model used for the investigation and that the combined use of different models provides a more solid informative basis about compound activity with implications for the mode of action of the studied drugs. Especially spheroid cultures mimicking the in vivo situation more closely should be included in any in vitro drug testing.

Conflict of interest The authors declare that they have no conflict of interest.

Authorship contributions Participated in research design: Ekaterina Schreiber-Brynzak, Simone Göschl, Robert Trondl, Helmut Dolznig, Michael A. Jakupec, Bernhard K. Keppler

Conducted experiments: Ekaterina Schreiber-Brynzak, Erik Klapproth, Christine Unger, Irene Lichtscheidl-Schultz, Sarah Schweighofer

Performed data analysis: Ekaterina Schreiber-Brynzak, Erik Klapproth, Simone Göschl, Christine Unger

Wrote or contributed to the writing of the manuscript: Ekaterina Schreiber-Brynzak, Christine Unger, Simone Göschl, Michael A. Jakupec

References

1. Unger C, Kramer N, Walzl A, Scherzer M, Hengstschläger M, Dolznig H (2014) Modeling human carcinomas: physiologically relevant 3D models to improve anti-cancer drug development. Adv Drug Deliv Rev 79–80:50–67
2. Sutherland RM (1988) Cell and environment interactions in tumor microregions: the multicell spheroid model. Science 240(4849): 177–184
3. Friedrich J, Ebner R, Kunz-Schughart LA (2007) Experimental anti-tumor therapy in 3-D: spheroids-old hat or new challenge? Int J Radiat Biol 83(11–12):849–871
4. Hirschhaeuser F, Menne H, Dittfeld C, West J, Mueller-Klieser W, Kunz-Schughart LA (2010) Multicellular tumor spheroids: an underestimated tool is catching up again. J Biotechnol 148(1):3–15
5. Kim H, Phung Y, Ho M (2012) Changes in global gene expression associated with 3D structure of tumors: an ex vivo matrix-free mesothelioma spheroid model. PLoS One 7(6), e39556
6. Mehta G, Hsiao AY, Ingram M, Luker GD, Takayama S (2012) Opportunities and challenges for use of tumor spheroids as models to test drug delivery and efficacy. J Control Release 164(2):192–204
7. Durand RE, Olive PL (2001) Resistance of tumor cells to chemo- and radiotherapy modulated by the three-dimensional architecture of solid tumors and spheroids. Methods Cell Biol 64:211–233
8. Desoize B, Jardillier JK (2000) Multicellular resistance: a paradigm for clinical resistance? Crit Rev Oncol Hematol 36(2–3):193–207
9. Shannon AM, Bouchier-Hayes DJ, Condron CM, Toomey D (2003) Tumour hypoxia, chemotherapeutic resistance and hypoxia-related therapies. Cancer Treat Rev 29(4):297–307
10. Bertout JA, Patel SA, Simon MC (2008) The impact of O2 availability on human cancer. Nat Rev Cancer 8(12):967–975
11. Brown JM (1999) The hypoxic cell: a target for selective cancer therapy—eighteenth Bruce F. Cain Memorial award lecture. Cancer Res 59:5863–5870
12. Ma HL, Jiang Q, Han S, Wu Y, Cui Tomshine J, Wang D, Gan Y, Zou G, Liang XJ (2012) Multicellular tumor spheroids as an in vivo–like tumor model for three-dimensional imaging of chemotherapeutic and nano material cellular penetration. Mol Imaging 11(6):487–498
13. Trédan O, Galmarini CM, Patel K, Tannock IF (2006) Drug resistance and the solid tumor microenvironment. Nat Rev Cancer 6(8): 583–592
14. Phillips RM, Loadman PM, Cronin BP (1998) Evaluation of a novel in vitro assay for assessing drug penetration into avascular regions of tumours. Br J Cancer 77(12):2112–2119
15. Wilson WR, Hay MP (2011) Targeting hypoxia in cancer therapy. Nat Rev Cancer 11(6):393–410
16. Semenza GL (2012) Molecular mechanisms mediating metastasis of hypoxic breast cancer cells. Trends Mol Med 18(9):534–543
17. Chang Q, Jurisica I, Do T, Hedley DW (2011) Hypoxia predicts aggressive growth and spontaneous metastasis formation from orthotopically grown primary xenografts of human pancreatic cancer. Cancer Res 71(8):3110–3120
18. Vaupel P (2009) Prognostic potential of the pre-therapeutic tumor oxygenation status. Adv Exp Med Biol 645:241–246
19. Nagelkerke A, Bussink J, Mujcic H, Wouters BG, Lehmann S, Sweep FC, Span PN (2013) Hypoxia stimulates migration of breast cancer cells via the PERK/ATF4/LAMP3-arm of the unfolded protein response. Breast Cancer Res 15(1):R2
20. Tian X, Wang W, Zhang Q, Zhao L, Wei J, Xing H, Song Y, Wang S, Ma D, Meng L, Chen G (2010) Hypoxia-inducible factor-1α enhances the malignant phenotype of multicellular spheroid HeLa cells in vitro. Oncol Lett 1(5):893–897
21. Korch C, Spillman MA, Jackson TA, Jacobsen BM, Murphy SK, Lessey BA, Jordan VC, Bradfrod AP (2012) DNA profiling analysis of endometrial and ovarian cell lines reveals misidentification, redundancy and contamination. Gynecol Oncol 127:241–248
22. Hart FA, Laming FP (1964) Complexes of 1,10-phenanthroline with lanthanide chlorides and thiocyanates. J Inorg Nucl Chem 26:579–585
23. Peti W, Pieper T, Sommer M, Keppler BK, Giester G (1999) Synthesis of tumor-inhibiting complex salts containing the anion trans-tetrachlorobis(indazole)ruthenate(III) and crystal structure of the tetraphenylphosphonium salt. Eur J Inorg Chem 1551–1555
24. Collery P, Jakupec MA, Kynast B, Keppler BK (2006) Preclinical and early clinical development of the antitumor gallium complex KP46 (FFC11). In: Alpoim MC, Morais PC, Santos MA, Cristóvão AJ, Centeno JA, Collery P (eds.) Metal ions in biology and medicine 9: 521–524
25. Abramkin SA, Jungwirth U, Valiahdi SM, Dworak C, Habala L, Meelich K, Berger W, Jakupec MA, Hartinger CG, Nazarov AA, Galanski M, Keppler BK (2010) {(1R,2R,4R)-4-methyl-1,2-cyclohexanediamine}oxalatoplatinum(II): a novel enantiomerically pure oxaliplatin derivative showing improved anticancer activity in vivo. J Med Chem 53:7356–7364
26. Dhara SC (1970) Rapid method for the synthesis of cis-[Pt(NH3)2Cl2]. Indian J Chem 8:193–194
27. Kidani Y, Inagaki K, Iigo M, Hoshi A, Kuretani K (1978) Antitumor activity of 1,2-diaminocyclohexane–platinum complexes against sarcoma-180 ascites form. J Med Chem 21:1315–1318
28. Albini A, Iwamoto Y, Kleinman HK (1987) A rapid in vitro assay for quantitating the invasive potential of tumor cells. Cancer Res 47(12):3239–3245
29. Vinci M, Gowan S, Boxall F, Patterson L, Zimmermann M, Court W, Lomas C et al (2012) Advances in establishment and analysis of three-dimensional tumor spheroid-based functional assays for target validation and drug evaluation. BMC Biol 10(1):29
30. Liu WD, Zhang T, Wang CL, Meng HM, Song YW, Zhao Z, Li ZM (2012) Sphere-forming tumor cells possess stem-like properties in human fibrosarcoma primary tumors and cell lines. Oncol Lett 4(6): 1315–1320
31. Bjørge L, Junnikkala S, Kristoffersen EK, Hakulinen J, Matre R, Meri S (1997) Resistance of ovarian teratocarcinoma cell spheroids to complement-mediated lysis. Br J Cancer 75(9):1247–1255
32. Laurent J, Frongia C, Cazales M, Mondesert O, Ducommun B, Lobjois V (2013) Multicellular tumor spheroid models to explore cell cycle checkpoints in 3D. BMC Cancer 13:73
33. Ke Q, Costa M (2006) Hypoxia-inducible factor-1 (HIF-1). Mol Pharmacol 70(5):1469–1480
34. Maxwell PH, Dachs GU, Gleadle JM, Nicholls LG, Harris AL, Stratford IJ, Hankinson O, Pugh CW, Ratcliffe PJ (1997) Hypoxia-inducible factor-1 modulates gene expression in solid

tumors and influences both angiogenesis and tumor growth. Proc Natl Acad Sci U S A 94:8104–8109
35. Hofheinz RD, Dittrich C, Jakupec MA, Drescher A, Jaehde U, Gneist M, Graf von Keyserlingk N, Keppler BK, Hochhaus A (2005) Early results from a phase I study on orally administered tris(8-quinolinolato)gallium(III) (FFC11, KP46) in patients with solid tumors—a CESAR study (Central European Society for Anticancer Drug Research – EWIV). Int J Clin Pharmacol Ther 43(12):590–591
36. Collery P, Domingo JL, Keppler BK (1996) Preclinical toxicology and tissue gallium distribution of a novel antitumour gallium compound: tris(8-quinolinolato)gallium (III). Anticancer Res 16:687–692
37. Thompson DS, Weiss GJ, Jones SF, Burris HA, Ramanathan RK, Infante RJ, Bendell JC, Ogden A, Von Hoff DD (2012) NKP-1339: maximum tolerated dose defined for first-in-human GRP78 targeted agent. J Clin Oncol 30, Suppl., abstr. 3033
38. Bergamo A, Masi A, Jakupec MA, Keppler BK, Sava G (2009) Inhibitory effects of the ruthenium complex KP1019 in models of mammary cancer cell migration and invasion. Met-Based Drugs 681270
39. Dolznig H, Rupp C, Puri C, Haslinger C, Schweifer N, Kerjaschki D, Garin-Chesa P (2011) Modeling adenocarcinomas in vitro: a novel 3D co-culture system induces cancer relevant pathways upon tumour-stroma interaction. Am J Path 179(1):487–501
40. Hinz B, Celetta G, Tomasek JJ, Gabbiani G, Chaponnier C (2001) Alpha-smooth muscle actin expression upregulates fibroblast contractile activity. Mol Biol Cell 12(9):2730–2741
41. Christian MM, Moy RL, Wagner RF, Yen-Moore A (2001) A correlation of alpha-smooth muscle actin and invasion in micronodular basal cell carcinoma. Dermatol Surg 27(5):441–445
42. de Wever O, Demetter P, Mareel M, Brack M (2008) Stromal myofibroblasts are drivers of invasive cancer growth Int. J Cancer 123:2229–2238
43. Valiahdi SM, Heffeter P, Jakupec MA, Marculescu R, Berger W, Rappersberger K, Keppler BK (2009) The gallium complex KP46 exerts strong activity against primary explanted melanoma cells and induces apoptosis in melanoma cell lines. Melanoma Res 19(5): 283–293
44. Desoize B, Collery P, Akéli JC, Keppler B (2000) Tris(8-quinolinolato)Ga(III) is active against unicellular and multicellular resistance. Met Ions Biol Med 6:573–576
45. Carlsson J, Nederman T (1989) Tumour spheroid technology in cancer therapy research. Eur J Cancer 25(8):1127–1133
46. Hazlehurst LA, Dalton WS (2001) Mechanisms associated with cell adhesion mediated drug resistance (CAM-DR) in hematopoietic malignancies. Cancer Metastasis Rev 20(1–2):43–50
47. Erler JT, Cawthorne CJ, Williams KJ, Koritzinsky M, Wouters BG, Wilson C, Miller C, Demonacos C, Stratford IJ, Dive C (2004) Hypoxia-mediated down-regulation of Bid and Bax in tumors occurs via hypoxia-inducible factor 1-dependent and –independent mechanisms and contributes to drug resistance. Mol Cell Biol 24: 2875–2889
48. Enyedi ÉA, Dömötör O, Bali K, Hetényi A, Tuccinardi T, Keppler BK (2015) Interaction of the anticancer gallium(III) complexes of 8-hydroxyquinoline and maltol with human serum proteins. J Biol Inorg Chem 20:77–88
49. Rainaldi G, Calcabrini A, Arancia G, Santini MT (1999) Differential expression of adhesion molecules (CD44, ICAM-1 and LFA-3) in cancer cells grown in monolayer or as multicellular spheroids. Anticancer Res 19(3A):1769–1778
50. Jungwirth U, Gojo J, Tuder T, Walko G, Holcmann M, Schöfl T, Nowikovsky K, Wilfinger N, Schoonhoven S, Kowol CR, Lemmens-Gruber R, Heffeter P, Keppler BK, Berger W (2014) Calpain-mediated integrin deregulation as a novel mode of action for the anticancer gallium compound KP46. Mol Cancer Ther 13(10):2436–2449
51. Heffeter P, Jakupec MA, Körner W, Wild S, von Keyserlingk NG, Elbling L, Zorbas H, Korynevska A, Knasmüller S, Sutterlüty H, Micksche M, Keppler BK, Berger W (2006) Anticancer activity of the lanthanum compound [tris(1,10-phenanthroline)lanthanum(III)]trithiocyanate (KP772; FFC24). Biochem Pharmacol 71(4):426–440
52. Trondl R, Heffeter P, Kowol CR, Jakupec MA, Berger W, Keppler BK (2014) NKP-1339, the first ruthenium-based anticancer drug on the edge to clinical application. Chem Sci 5:2925–2932
53. Heffeter P, Atil B, Kryeziu K, Groza D, Koellensperger G, Körner W, Jungwirth U, Mohr T, Keppler BK, Berger W (2013) The ruthenium compound KP1339 potentiates the anticancer activity of sorafenib in vitro and in vivo. Eur J Cancer 49(15):3366–3375
54. Bytzek AK, Boeck K, Hermann G, Hann S, Keppler BK, Hartinger CG, Koellensperger G (2011) LC- and CZE-ICP-MS approaches for the in vivo analysis of the anticancer drug candidate sodium trans-[tetrachloridobis(1H-indazole)ruthenate(III)] (KP1339) in mouse plasma. Metallomics 3(10):1049–1055
55. Dömötör O, Hartinger CG, Bytzek AK, Kiss T, Keppler BK, Enyedy EA (2013) Characterization of the binding sites of the anticancer ruthenium(III) complexes KP1019 and KP1339 on human serum albumin via competition studies. J Biol Inorg Chem 18(1):9–17
56. Roberts DL, Williams KJ, Cowen RL, Barathova M, Eustace AJ, Brittain-Dissont S, Tilby MJ, Pearson DG, Ottley CJ, Stratford IJ, Dive C (2009) Contribution of HIF-1 and drug penetrance to oxaliplatin resistance in hypoxic colorectal cancer cells. Br J Cancer 101(8):1290–1297